Electron density distribution in paramagnetic and antiferromagnetic NiO: A γ-ray diffraction study

W. Jauch
Hahn-Meitner-Institut, Glienicker Strasse 100, D-14109 Berlin, Germany

M. Reehuis
Max-Planck-Institut für Festkörperforschung, Heisenbergstrasse 1, D-70569 Suttgart, Germany
(Received 8 June 2004; published 29 November 2004)

High-accuracy single-crystal structure factor data sets, complete up to $\sin\theta/\lambda = 1.6$ Å^{-1}, have been measured from paramagnetic NiO at 550 K and in the antiferromagnetic state at 10 K using 316.5 keV gamma radiation. In the rhombohedral low-temperature phase, monodomain formation was enforced by application of moderate stress. A detailed description of the electron density distribution is derived in terms of a multipolar atomic deformation model. Pronounced asphericity is found in the nickel valence region which, unexpectedly, is not significantly influenced by the magnetic order. NiO thus exhibits a radically different behavior than that found for MnO or CoO. Similarly, very different charge responses of the e_g and t_{2g} subshells in the paramagnetic states are observed, supporting a prediction from theory. The 3*d* charge distribution is contracted by about 3% relative to the free atom; the total number of *d* electrons on nickel amounts to 7.65(1). From the 3*d* population analysis, unquenched orbital angular momentum is derived, in quantitative accordance with magnetic x-ray measurements. Electronic properties at the bond critical points reveal the Ni-O interactions as purely ionic. Methodological issues such as the importance of high momentum data and the influence of the wave-function quality are also discussed.

DOI: 10.1103/PhysRevB.70.195121 PACS number(s): 71.20.−b, 61.50.Lt

I. INTRODUCTION

NiO is generally considered as the prototype of antiferromagnetic Mott insulators and is one of the most thoroughly studied materials. The ground-state electron density is a well-defined observable that plays a fundamental role in the theory of the solid state in view of its tight connection to energy, as expressed by the Hohenberg-Kohn theorem. The present paper is aimed at an accurate determination of the spatial distribution of the electronic charge density in the unit cell of paramagnetic and antiferromagnetic NiO through Bragg γ-ray diffraction. The charge distribution is described in terms of atomic positional, thermal vibrational, and electronic charge parameters. These parameters are then fitted by least squares to the observed structure factors, i.e., the Fourier components of the electron density in the crystal. At first glance, it may appear to be surprising that no high-resolution x-ray diffraction measurements on single crystals of NiO have been reported so far. Despite the simplicity of the structure, several experimental problems must be overcome which are related to the occurrence of domains in the ordered phase and to the elevated temperature required to investigate the paramagnetic phase. Electron diffraction has been employed to measure seven low-order structure factors at 110 K,[1] but this is insufficient to extract the charge density distribution in the solid. The present work is a follow up to previous γ-ray diffraction studies of CoO and MnO.[2,3]

With the use of 316 keV gamma radiation, the high energy diffraction case (photon energy » binding energy of K-shell electrons) is fully realized so that less corrections and fewer assumptions must be made in the process of deriving structure factors from the observed integrated intensities, and a structure factor accuracy below the 0.1% level is achievable. No highly uncertain dispersion corrections for the heavier atoms need to be applied. The improvement in accuracy is not solely a consequence of the high photon energy but is also brought about by additional favorable experimental conditions, such as the perfect stability, homogeneity and spectral linewidth ($\Delta\lambda/\lambda = 10^{-6}$) of the incident γ-ray beam. There are thus important advantages to the diffraction conditions met in synchrotron radiation work as far as systematic error sources are concerned.[4]

II. CRYSTAL STRUCTURE

Paramagnetic NiO has the NaCl structure (space group $Fm\bar{3}m$; $a = 4.190\,56$ Å at 550 K).[5] The transition to the antiferromagnetic state at $T_N = 523$ K is accompanied by a rhombohedral distortion with a contraction of the cubic unit cell along the ⟨111⟩ axes. The resulting crystallographic symmetry is trigonal (space group $R\bar{3}m$). At 10 K, the rhombohedral cell parameters are $a = 2.9490$ Å, $\alpha = 60.087°$.[5] Note that the rhombohedral contraction in NiO is an order of magnitude smaller than in antiferromagnetic MnO. For the present purpose, it is more convenient to use a hexagonal unit cell (three times the volume of the primitive rhombohedral cell) with the lattice constants $a = 2.9529$ Å and $c = 7.2188$ Å, and with Ni at $3a$ $(0,0,0)$ and O at $3b$ $(0,0,1/2)$. Since the direction of the sublattice magnetization is perpendicular to the triad axis, the true symmetry must be lower than trigonal. No monoclinic splitting of reflections in the diffraction pattern has been perceptible so far, indicating the additional distortion to be extremely small.

III. EXPERIMENTAL AND DATA REDUCTION

The single crystal used in the present investigation was a cuboid of dimensions $3.04\times3.18\times3.34$ mm^3 with {111} surfaces, purchased from MaTecK/Jülich (Germany). The diffraction data have been collected on the gamma-ray diffractometer installed at the Hahn-Meitner-Institut where the most intense line of an ^{192}Ir source ($T_{1/2}=73.83$ d) with a wavelength of 0.0392 Å (316.5 keV) is used. The diffracted gamma rays were recorded in ω-step scan mode with an intrinsic germanium detector.

Data sets, complete up to $\sin\theta/\lambda=1.6$ Å^{-1}, were collected at 550 K [high temperature (HT)] and at 10 K [low temperature (LT)]. Profile fits of the rocking curves at both temperatures revealed a Gaussian shape with a full width at half-maximum (FWHM) of 4.8 minutes of arc, which is broader than the incident beam divergence with a FWHM of 3.2 minutes of arc. The crystal mosaic distribution is thus of a Gaussian type with a FWHM of 3.6 minutes of arc.

Below T_N, crystallographic domains can occur, resulting from twinning of the crystal according to the four equivalent [111] contraction axes. At LT, the sample was forced into a monodomain by [111] stress of approximately 140 bar, applied through aluminium plates driven by a steel spring thereby also reducing thermal stress during the cooling down process. Aluminium foil was inserted between sample and aluminum plate further ensuring constant stress conditions. The assembly was heated up to 100 degrees above T_N before cooling below the phase transition.

An absorption correction was carried out ($\mu=0.709$ cm^{-1}), resulting in a transmission range from 0.794 to 0.816. At HT, 390 diffraction data were measured corresponding to 93 independent reflections with an unprecedented counting-statistical overall precision of $\Sigma\sigma(I)/\Sigma I=0.0038$ for the averaged data. At LT, 769 observations merged into 251 independent data with $\Sigma\sigma(I)/\Sigma I=0.0080$. The absorption-weighted mean path lengths through the sample varied between 2.83 mm and 3.25 mm. It was therefore considered necessary to process each reflection with its individual path length in the calculation of the extinction correction, and to treat symmetrically equivalent reflections separately. Data reduction was carried out using the XTAL suite of crystallographic programs.[6]

The HT data were corrected for the contribution of inelastic thermal diffuse scattering (TDS) to the total intensity. The formalism of Skelton and Katz[7] was applied, using the elastic constants from Hearmon[8] and the instrumental parameters defining the sampled volume in reciprocal space: ω-scan peak width=0.4°, full circular detector window=0.46°. The maximum TDS contribution was 10%.

IV. RESULTS

Structure refinements were performed with the program system VALRAY,[9] minimizing $\chi^2=\Sigma w(|F_o|^2-|F_c|^2)^2$, where F_o and F_c are the observed and calculated structure factors, respectively. The observations were weighted solely by their counting-statistical variances.

A. Independent-atom model

Scattering factors for neutral Ni and O atoms were calculated from the Hartree-Fock wave functions given in Clementi and Roetti.[10] The fit parameters were the scale factor of the observed sructure factors, a secondary extinction parameter using the Becker-Coppens formalism,[11] and the mean square vibrational amplitudes of the two atoms. In order to reduce the influence of charge-density deformations in the outer shells, high-order refinements were carried out, taking into account only reflections with $\sin\theta/\lambda>0.7$ Å^{-1}. The resulting scale factor was fixed in later refinements with improved scattering models. To test for deviations from ideal stoichiometry, in particular, for metal deficiency, the occupancy of the nickel site was allowed to vary in a high-order refinement, resulting in an ideal value of 1.03(3), with scale and thermal parameters being fitted simultaneously [fixing the scale factor yields 1.0006(10)].

The chi-square of the high-order fits showed scope for improvement. It has therefore been checked whether the data are compatible with the allowance of internal degrees of freedom in the LT trigonal lattice. The following three possible cases have been considered: trigonal setting $R\bar{3}m$ with $c'=2c$ (Ni:$3a$,$3b$;O:$6c$), monoclinic setting $I\,1\,2/m\,1$ (Ni:$2a$;O:$2d$) and triclinic setting $P\bar{1}$ (Ni:$2i$;O:$2i$). In all cases, the additional parameters turned out to be virtually identical with the high-symmetry values.

The hypothesis that a small fraction of the metal atoms occupies not the octahedral positions but rather the interstitial tetrahedral sites of the HT rocksalt structure was also examined. The analysis followed the lines given by Roth.[12] The refined occupancy numbers of the octahedral and tetrahedral sites were found to be 1.0029(23) and −0.0029(23), respectively, so that the disorder model is clearly refuted. Both accepted structures of NiO have thus been fully confirmed. It was later realized that the high accuracy of the high-order data was simply not exhausted by the IAM, but required the inclusion of additional effects through a more sophisticated scattering model.

B. Multipole model

In the aspherical atom multipole model the electron density distribution is projected onto a small finite basis set of real spherical harmonic functions centered at the nuclear positions with the local density rigidly following the motion of its associated nucleus.[13] For nickel, the atomic density is represented as

$$\rho_{\mathrm{Ni}}(\mathbf{r})=\rho_{\mathrm{Ni,core}}(r)+\kappa^3R_{3d}(\kappa r)\sum_{l=0}^{4}\sum_{m=0}^{l}P_{lm\pm}y_{lm\pm}(\mathbf{r}/r).$$

With the site symmetry $m\bar{3}m$ of the rocksalt structure the only allowed higher multipole is the fourth order cubic harmonic which is a linear combination of y_{40} and y_{44+}. In the rhombohedral phase the site symmetry is $\bar{3}m$ and the contributing multipoles are $(l,m)=(0,0)$, (2,0), (4,0), $(4,3+)$.

TABLE I. Quality of fit for the various scattering models; *Np* = number of adjustable parameters. Number of reflections: 390 at 550 K and 769 at 10 K. In all cases, the scale factor was fixed to the value obtained from high-order IAM refinements.

		IAM	Monopoles	Multipoles
$T=550$ K	χ^2	3555	2554	965
	Np	3	6	8
$T=10$ K	χ^2	4726	3661	2023
	Np	5	8	14

For oxygen,

$$\rho_O(\mathbf{r}) = \rho_{O,core}(r) + P_{O,valence}\kappa^3\rho_{O,valence}(\kappa r) + \sum_{l=2}^{4}\kappa^3 R_l(\kappa r)\sum_{m=0}^{l} P_{lm\pm}y_{lm\pm}(\mathbf{r}/r).$$

$\rho_{Ni,core}$, $\rho_{O,core}$, and $\rho_{O,valence}$ are unperturbed HF electron densities of the appropriate atomic orbitals. $\rho_{O,valence}$ is the average of the 2*s* and 2*p* orbitals, normalized to one electron. For Ni, the square of the radial part of the 3*d* canonical HF orbitals is used to construct both monopole and multipoles. Since the 4*s* valence electrons contribute very little to the scattering their population cannot be reliably determined, and their number is fixed to 2. The radial function for the $l=2$ pole of oxygen consists of a $2p2p$ atomic orbital product. The $l=4$ radial function of oxygen is a single Slater function, $r^4\exp(-\alpha r)$, with the standard exponent $\alpha=4.50$ Bohr^{-1}. The κ parameters allow for expansion ($\kappa<1$) or contraction ($\kappa>1$) of the radial functions. $P_{O,valence}$ and $P_{lm\pm}$ are variable population coefficients. Monopolar populations were constrained to ensure electroneutrality of the crystal. The spherical harmonics are expressed relative to a global Cartesian frame which is oriented parallel to the unit cell axes for the cubic phase. In the hexagonal cell, the *z* axis is along the principal symmetry axis [001], the *x* axis is along [210] and *y* is chosen along [010] so that one of the ligands lies in the *xz* plane. The y_{43+} multipole function is defined with positive lobes pointing towards the ligand atoms.

In Table I, the quality of fit is given for the various scattering models. The drastic reduction in χ^2 shows that the data strongly supports the multipole model, also to be reflected by the very narrow confidence limits on most fit parameters. A large improvement of fit is already obtained with a spherical atom model using only two charge parameters per atom, charge transfer and valence-shell expansion-contraction. The very high precision of the HT data is reflected by the large value of χ^2 for the IAM. The results of the multipole refinements are listed in Table II [$R(F)=0.0071$ and 0.0080 for HT and LT, respectively]. Note that the normalization condition for the aspherical density functions is such that the coefficients $P_{lm\pm}$ correspond to the local electrostatic moments in Å units.

Adjustment of the secondary extinction parameter gives $g=553(7)$ rad^{-1} for HT, in fair agreement with the observed value ($g=630$ rad^{-1}). For LT, $g=478(8)$ rad^{-1} is obtained.

TABLE II. Results from multipole refinements of paramagnetic and antiferromagnetic NiO. $U_\parallel$ and $U_\perp$ denote mean square vibrational amplitudes parallel and perpendicular to the threefold axis.

		550 K	10 K
Ni	$U_\parallel$(Å^2)	0.00625(1)	0.00146(1)
	$U_\perp$(Å^2)	0.00625(1)	0.00142(1)
	κ	1.033(2)	1.030(1)
	$P_{00}(\lvert e\rvert)$	7.63(2)	7.65(1)
	$P_{20}(\lvert e\rvert$Å$^2)$		−0.03(2)
	$P_{40}(\lvert e\rvert$Å$^4)$	−0.50(1)	0.28(2)
	$P_{43+}(\lvert e\rvert$Å$^4)$		−1.71(6)
O	$U_\parallel$(Å^2)	0.00704(4)	0.00271(7)
	$U_\perp$(Å^2)	0.00704(4)	0.00243(4)
	κ	0.973(2)	0.974(2)
	$P_{valence}(\lvert e\rvert)$	6.37(2)	6.35(1)
	$P_{20}(\lvert e\rvert$Å$^2)$		−0.16(4)
	$P_{40}(\lvert e\rvert$Å$^4)$	0.17(4)	−0.38(5)
	$P_{43+}(\lvert e\rvert$Å$^4)$		0.94(19)

Extinction factors are listed in Table III for the lowest-order HT structure factors that have been measured to a statistical precision well below 0.1%. The quantitative agreement between observed and fitted values is very good, strongly indicating that extinction has been treated properly.

The static model densities, with the Debye-Waller factor omitted, were evaluated in direct space and checked for unphysical negative densities; they proved to be positive everywhere in the unit cell. Figures 1 and 2 show the static deformation densities (aspherical components only) calculated in direct space. The observed features are very pronounced, exhibiting magnitudes up to 7 eÅ^{-3}. The deformation maps will be further discussed below.

C. Characterization of the atomic interactions

The quantum theory of atoms in molecules (AIM)[14] provides a powerful interpretive tool which allows for a clear

TABLE III. Observed and calculated values of low-order structure factors of NiO in units of electrons per cell ($T=550$ K), extinction corrections applied to F_o. The extinction coefficients *y* refer to the reduction in F^2.

hkl	F_o	F_c	$\sigma(F_o)/F_o$	*y*
111	63.59(3)	63.52	0.05%	0.966
200	100.25(2)	100.24	0.02%	0.929
220	79.93(3)	80.06	0.04%	0.968
311	47.59(4)	47.36	0.08%	0.990
222	66.86(5)	66.99	0.07%	0.982
400	56.96(4)	56.92	0.07%	0.988

$R(F)=\Sigma\lvert F_o-F_c\rvert/\Sigma\lvert F_o\rvert=0.0015$
$R(\sigma)=\Sigma\sigma(F_o)/\Sigma\lvert F_o\rvert=0.0005$

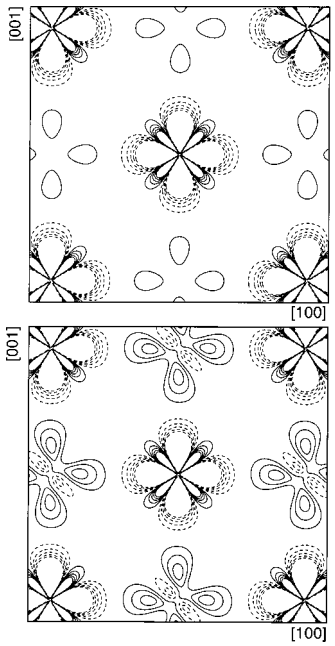

FIG. 1. Aspherical contributions to the static model density in the cubic (100) plane. Top: paramagnetic NiO with a density range from −7.10 to 1.78 eÅ^{-3}. Bottom: antiferromagnetic NiO with a density range from −6.19 to 1.57 eÅ^{-3}. Ni is located in the center and the corners of the maps. Solid lines represent positive regions, dashed lines represent negative regions in steps of 0.05 eÅ^{-3}. The zero contour is omitted. The densities are truncated at ±0.25 eÅ^{-3}.

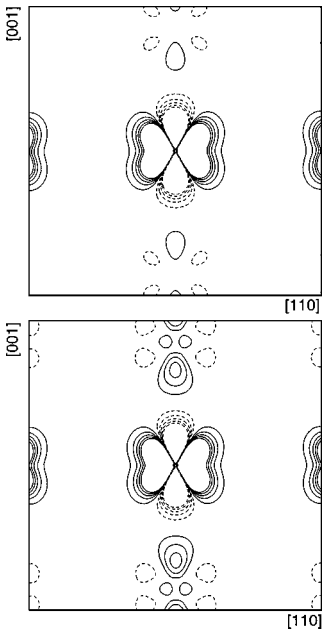

FIG. 2. Aspherical contributions to the static model density in the cubic (110) plane. Top: paramagnetic NiO with a density range from −6.98 to 4.72 eÅ^{-3}. Bottom: antiferromagnetic NiO with a density range from −6.10 to 4.25 eÅ^{-3}. Ni is located in the center of the map. Contours as in Fig. 1.

and rigorous characterization of the atomic interactions. The local properties of $\rho(\mathbf{r})$ at the bond critical saddle point, $\mathbf{r}_c$, signify the particular type of interaction between a bonded pair of atoms. An ionic bond is associated with a local charge depletion which is characterized by a positive Laplacian $\nabla^2\rho(\mathbf{r}_c)$ and a low value of $\rho(\mathbf{r}_c)$. The Laplacian is related to the electronic kinetic and potential energy densities, $G(\mathbf{r})$ and $V(\mathbf{r})$, respectively, by the local virial theorem, $(\hbar^2/4m)\nabla^2\rho(\mathbf{r})=2G(\mathbf{r})+V(\mathbf{r})$. At $\mathbf{r}_c$, the kinetic energy per electron, $G(\mathbf{r}_c)/\rho(\mathbf{r}_c)$, should be less than unity for covalent interaction but larger than unity for ionic interactions (when expressed in atomic units).

The characteristics of the bond critical points of the static model electron density are listed in Table IV. $G(\mathbf{r}_c)$ was obtained from a gradient expansion around the Hartree-Fock result for the homogeneous electron gas which is a suitable approximation in the internuclear region where $\rho(\mathbf{r})$ varies slowly: $G(\mathbf{r}_c)=2.8713[\rho(\mathbf{r}_c)]^{5/3}+0.16667\nabla^2\rho(\mathbf{r}_c)$ with all quantities expressed in atomic units.[15] The potential energy density can be estimated by combining this equation with the local virial theorem. From inspection of Table IV, the bonding state in NiO appears to be completely ionic. It is found that the total electronic energy density $H(\mathbf{r}_c)=G(\mathbf{r}_c)+V(\mathbf{r}_c)\cong 0$, a result which has also been obtained in our previous studies. In the case of a covalent bond, $H(\mathbf{r}_c)$ is dominated by $V(\mathbf{r}_c)$ and thus largely negative.[16] Concerning the ionic bonding interaction the situation is less clear and it is often asserted, according to Cremer *et al.*,[17] that in this case $G(\mathbf{r}_c)$ will dominate over $V(\mathbf{r}_c)$, thus leading to positive values of $H(\mathbf{r}_c)$. Our experimental results strongly suggest, however,

TABLE IV. Characteristics of the bond critical points in paramagnetic and antiferromagnetic NiO. $\lambda_{1,2,3}$ label the principal curvatures of $\rho(\mathbf{r}_c)$ with λ_3 being the component along the internuclear axis. Values of ρ in eÅ^{-3}, values of $\nabla^2\rho$ and λ_i in eÅ^{-5}. G, G/ρ, and V are given in atomic units.

$\mathbf{r}_c$	$\rho(\mathbf{r}_c)$	$\nabla^2\rho(\mathbf{r}_c)$	$\lambda_{1,2,3}$	$G(\mathbf{r}_c)$	$G(\mathbf{r}_c)/\rho(\mathbf{r}_c)$	$V(\mathbf{r}_c)$
$Fm\bar{3}m$						
0.2390(2), 0, 0	0.400(1)	7.25(1)	−1.15(1)	0.0761(1)	1.283(3)	−0.0769(3)
			−1.15(1)			
			9.55(3)			
$R\bar{3}m$						
0.348(2), 0.174(1), 0.412(1)	0.428(3)	7.52(2)	−1.49(5)	0.0809(4)	1.276(8)	−0.0839(8)
			−1.37(5)			
			10.38(8)			

the ionic bond to be characterized by the balance of the two local energy densities.

The AIM theory provides a unique partitioning of the total charge density into mononuclear regions, termed atomic basins (Ω), which are bound by a surface whose flux of the gradient vector field $\nabla\rho(\mathbf{r})$ vanishes. The electron population of an atom is obtained by integration of $\rho(\mathbf{r})$ over its basin. The net atomic charge, $q(\Omega)$, is the difference between the nuclear charge and the integrated electron population. Application of the algorithm by Flensburg and Madsen[18] gives $q(\mathrm{Ni}) = -q(\mathrm{O}) = 1.21|e|$, and $V(\mathrm{Ni}) = 8.77$ Å^3 and $V(\mathrm{O}) = 9.63$ Å^3. Again, the net atomic charges are considerably smaller than the formal value of 2. This observation is interesting since AIM charges are sometimes criticized for being too large in value compared with other methods.[19]

As already pointed out by the authors,[2,3] the absence of covalency is difficult to reconcile with the common understanding of the interatomic magnetic coupling in terms of the superexchange mechanism, rather, electron correlation should be taken into consideration.

V. DISCUSSION OF RESULTS

A. Vibrational parameters

It has been shown that the leading term of a high-temperature expansion ($T > \Theta_D$) of the Debye-Waller factor does not depend on the atomic masses but only on the interatomic forces, so that the heavier atoms do not necessarily have the smaller Debye-Waller values.[20] As a consequence, it follows for the rocksalt structure that if only nearest neighbor interaction is taken into account, both types of atoms should vibrate with equal amplitudes. From the two sound velocities the Debye temperature of NiO is estimated as $\Theta_D = 570$ K which is close to HT. The experimental result is $U(\mathrm{Ni})/U(\mathrm{O}) = 0.888(5)$. The two vibrational amplitudes are thus roughly the same in qualitative agreement with the lattice dynamical approximation. The result for cubic MnO, where the Debye-Waller factors turned out to be identical for both atoms, must therefore be regarded as a fortuitous coincidence.

At LT, the two atoms vibrate distinctly differently, approximately according to the square root of the inverse mass ratio. As in MnO, the vibrations along the threefold axis are larger than in the orthogonal plane: $U_{\parallel}/U_{\perp} = 1.12(3)$ for O, and 1.03(1) for Ni. The anisotropy ratio for the metal atom, however, is much smaller than in the other antiferromagnetic oxides.

Temperature dependent vibrational parameters for compounds with the NaCl structure have been calculated by Gao *et al.*[21] based on a semiempirical rigid ion model with parameters obtained from best fits to experimental phonon dispersion curves. The computational values for NiO are $U(\mathrm{Ni}) = 0.005\,95$ Å^2, $U(\mathrm{O}) = 0.007\,72$ Å^2 for HT, and $U(\mathrm{Ni}) = 0.001\,35$ Å^2, $U(\mathrm{O}) = 0.002\,76$ Å^2 for LT. Whereas the calculations give a too large difference between the HT values of the two atoms, the experimental LT values are reproduced quite well.

It has been checked whether the harmonic approximation for thermal motion is violated at HT. It turned out that multipole refinements with inclusion of the two symmetry-allowed quartic anharmonic terms in the Debye-Waller factors yielded only a minor improvement of fit. Both the physical and statistical significance of anharmonicity is thus only marginal in the present context.

B. Monopole parameters

Pronounced deviations from the independent-atom values are observed. The nickel valence shell is contracted by 3%, whereas the oxygen L shell exhibits an expansion of 2.6%. The expansion/contraction resembles that found in the previous studies, and is physically consistent with the observed charge transfer.

The valence electron population of oxygen is 6.35, corresponding to a net donation of 0.35 electrons from the nickel atom. The observed invariance of the refined monopole parameters with respect to the magnetic phase is an important physical constraint, and its fulfillment at a highly quantitative level reflects the accuracy that has actually been achieved.

The total number of d electrons on Ni is found to be significantly smaller than the formal value of 8. The Ni ground state has been estimated from a cluster model to be an admixture of 82% $3d^8$ and 18% $3d^9L$, where L represents a hole on the oxygen ligand.[22] This estimate is not supported by the present work.

Information about the spatial extent of the unpaired electrons can also be obtained from magnetic neutron diffraction. In the 1960s, the magnetic form factor of Ni in NiO was determined using magnetic Bragg scattering of unpolarized neutrons, and it was found that the unpaired electrons are considerably contracted compared to the free atom.[23] It was later shown that about 4% of the 17% contraction is only apparent and can be accounted for the scattering from the residual orbital moment.[24] The use of unpolarized neutron data is involved with large uncertainties and the above value must be regarded only as a crude estimate. Note that the classical polarized neutron technique cannot be applied to antiferromagnetic NiO since nuclear and magnetic scattering do not coincide in mixed reflections. In a theoretical form factor study[25] a much reduced value of 4% was obtained for the spatial contraction of Ni which comes close to the present experimental result.

C. *d*-orbital populations and magnetic moments

The $3d$ electron density may be described by multipole functions or, alternatively, it may be expressed in terms of the atomic orbitals d_i. There is a linear relationship between the multipole population and the d-orbital population coefficients.[26] In the cubic crystal field, the d orbitals split into doublet e_g orbitals pointing towards the ligands and the lower-lying triplet t_{2g} orbitals pointing between them.

On the lowering of the symmetry from cubic to trigonal, the t_{2g} orbitals split into a single a_g with its lobes pointing along the threefold axis and a doubly degenerate e_g level, whereas the original e_g orbitals retain their symmetry characteristics and are now termed e_g'. The four multipole parameters transform into three population factors and a mixed product term $e_g\, e_g'$ (see Ref. 3 for more details). The calcu-

TABLE V. 3*d*-orbital populations on Ni; in the hexagonal cell *z* is along [001] and *x* is chosen so that one of the ligands lies in the *xz* plane.

Orbital	$m\bar{3}m$	Orbital	$\bar{3}m$
e_g	2.00(3)	e_g'	2.17(3)
t_{2g}	5.64(4)	e_g	3.79(3)
		a_g	1.69(1)
		$e_g e_g'$	−0.24(3)
Total *d*	7.63(2)		7.65(1)

lated distributions of the *d* electrons over the orbitals are listed in Table V.

In the cubic crystal field the ratio of the e_g/t_{2g} population is found to be 0.354(6), rather close to the nominal 2:6 ratio corresponding to a spherical Ni atom. This result is completely different from that for MnO and CoO where the experimental e_g/t_{2g} ratios are considerably larger than the ideal ratios. Our results may be compared with recent theoretical work (LDA+*U* method[27]) where the response of the e_g and t_{2g} electrons to an applied potential shift has been investigated. The two subshells turn out to show a very different behavior. Whereas a positive potential shift always leads to a decrease in t_{2g} population, the influence on the e_g occupation is specific for the particular compound. For MnO and FeO, a corresponding increase in e_g occupation is found, but in NiO variation of the potential has no influence on the e_g electrons so that an occupation number of 2 is expected and the e_g/t_{2g} ratio should only be slightly larger than the spherical atom value. The theory-deduced behavior of the e_g electrons has been called counterintuitive,[27] but it has by now been shown to be a real effect, substantiated in detail by our diffraction experiment. The spherical atom populations for e_g and t_{2g} amount to 3.2 and 4.8 electrons, respectively. Therefore, in Figs. 1 and 2 (top) the e_g orbitals appear as lobes of depleted density, and the t_{2g} orbitals show up as peaks.

Considerable repartition of valence density, associated with magnetic ordering, was observed in MnO and CoO. Surprisingly, NiO shows a quite different behavior which might correlate with its significantly smaller rhombohedral distortion. From Figs. 1 and 2 (bottom) hardly any change is recognizable in the density surrounding Ni, whereas the features around oxygen clearly show a polarization of electron density towards the metal atom. The highly significant extent of e_g/e_g' orbital mixing demonstrates that cubic symmetry is indeed broken since otherwise it would have vanished.

From magnetic x-ray scattering an orbital-to-spin angular momentum ratio of $L/S=0.34(6)$ has been determined for NiO at 300 K (as compared to $L/S=3$ for the free atom).[28] The corresponding orbital magnetic moment amounts to $\mu_L=0.32(5)\mu_B$. From LSDA+*U* calculations follows $\mu_L=0.29\mu_B$ and $L/S=0.36$ in close agreement with the experimental values.[29] The e_g/e'_g mixing and the fractional orbital populations prevent a straightforward application of Hund's first rule to infer the spin magnetic moment. The orbital angular momentum is completely quenched for a doublet ground state.[30] Therefore no orbital momentum exists for the idealized $(t_{2g})^6(e_g)^2$ electron configuration of Ni. From the observed finite momentum it follows therefore that the unpaired electrons cannot be in a state of pure e_g symmetry. As evident from Table V, the a_g state is indeed only partially filled and gives rise to the magnetic moment $\mu_L=0.31(2)$. It is worthy to note that subtle magnetic properties can be extracted from charge density derived quantitative information.

From neutron diffraction the total magnetic moment, proportional to the sum $2S+L$, is accessible. An ordered moment of $1.90(6)\mu_B$ per nickel was obtained from powder diffraction.[31] To deduce the absolute moment, the zero-point spin deviation has to be taken into consideration. A correction of 7.6% has been found for NiO,[32] so that the absolute magnetic moment is $2.05\mu_B$, identical with the nominal integer spin-only value. In the absence of further information one could thus have erroneously concluded the orbital moment to be fully quenched in NiO. However, the localized spin moment is reduced to $\mu_S=1.7\mu_B$ instead. The spin reduction is consistent with the refined monopole charge on Ni. Finally, it is worth pointing out that in recent LDA+*U* calculations of electron-energy-loss spectra agreement with experiment could only be obtained with a reduced spin moment, $\mu_S=1.77\mu_B$, at the Ni atoms.[33]

VI. METHODOLOGICAL ASPECTS

A. Form factor dependence

As mentioned above, the present study uses the analytical expressions for nonrelativistic Hartree-Fock atomic wave functions by Clementi and Roetti. More recent compilations are due to Bunge *et al.*[34] To test the sensitivity of our results to the wave functions employed, the HT multipole fits have been repeated using the recent wave functions. The set of wave functions by Bunge *et al.* have improved energy accuracy but resulted in a dramatic deterioration of fit ($\Delta\chi^2=+40\%$ relative to the reference value from Table I). One must keep in mind that the diffraction experiment provides information on the electron density distribution so that energy- rather than density-optimized wavefunctions may turn out to be an inadequate choice for density modeling.

New analytical expressions for relativistic Dirac-Hartree-Fock wave functions of the core and valence electrons have been reported by Su and Coppens[35] promising a more accurate construction of free-atom form factors especially for heavier atoms. The relativistic wave functions from Ref. 35 lead to a slight improvement in quality of fit ($\Delta\chi^2=-2\%$). Use of the relativistic function for Ni but the Clementi-Roetti function for oxygen resulted in a further improvement ($\Delta\chi^2=-3\%$) which is of course inconsistent with the fully relativistic result.

A better approximation to the exact atomic Rayleigh scattering amplitudes than the ordinary form factor $f(q)$ is the modified relativistic form factor $g(q)$ which takes into account binding effects among the electrons and between electrons and nucleus.[36] It should be noted that $g(q)$ is no longer the Fourier transform of the electronic charge distribution.[36] For relativistic electrons the forward-scattering amplitude is reduced from the classically expected atomic number, $f(0)$

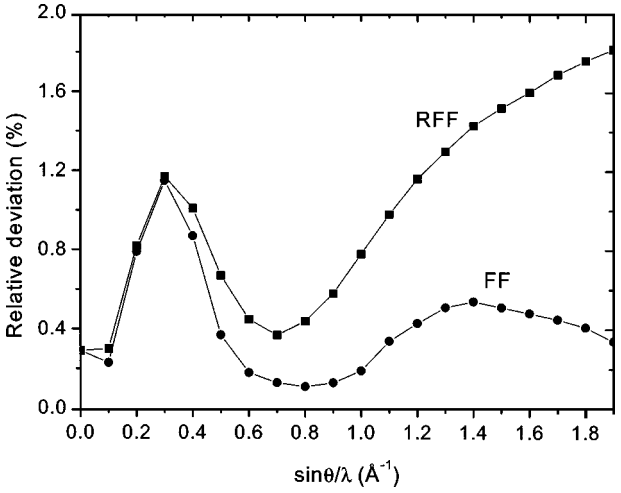

FIG. 3. Relative deviation, in percent, of the ordinary nonrelativistic (FF) and relativistic (RFF) form factors from the modified form factor for nickel.

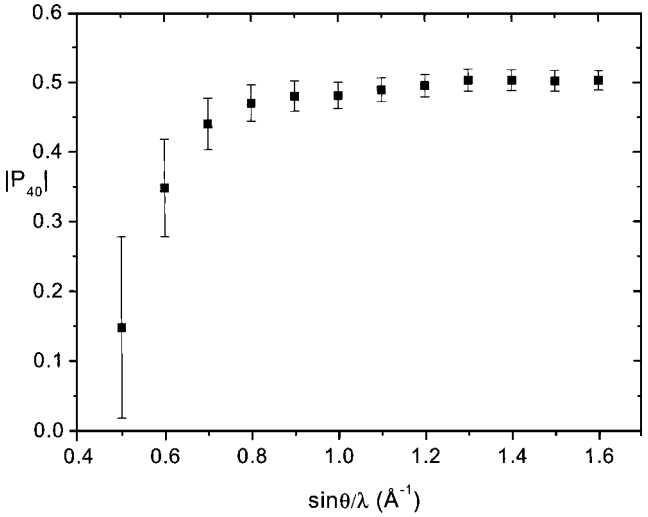

FIG. 4. The refined population P_{40}(Ni) at HT as a function of increasing momentum cutoff values.

$=Z$, to $g(0)=Z-|E_{\mathrm{tot}}|/mc^2$ (E_{tot}: total ground-state binding energy) due to the relativistic increase in mass of the core electrons. A complete tabulation of $g(q)$ is given by Schaupp *et al.*[37] The tables list the total-atom values but no shell-by-shell contributions which are essential for the present type of analysis. The influence of relativistic effects can therefore not be checked with the multipole-expansion formalism. Nevertheless, a comparison can be made of the three types of form factors, as presented in Fig. 3 for nickel. It illustrates that the form factor obtained from nonrelativistic wave functions comes closer to $g(q)$ than that from relativistic wave functions. At first sight this result seems to be surprising, but it rather represents a typical example of a compensation effect: the increase in scattering amplitude due to relativistic wave functions is almost entirely canceled by the genuine relativistic effect, the reduction due to binding. It is important to note that the disagreement between $g(q)$ and relativistic $f(q)$ increases with higher-Z elements. Nonrelativistic form factors computed from Clementi-Roetti wave functions are thus the most appropriate approximation to $g(q)$, which recommends their use. It is somehow ironical in this respect that only the relativistic $f(q)$ is tabulated in the *International Tables for Crystallography (Vol. C).*[38] One must be aware that the quality of the atomic form factors puts a limit on the accuracy in the determination of electron densities.

Finally, attention is paid to the effect of the nuclear Thomson amplitude. For Ni, $f_N=0.0073$, which amounts to 0.15% of the electronic contribution at the resolution limit, $\sin\theta/\lambda=1.6$ Å^{-1}. It is smaller than the other uncertainties and can be neglected.

B. Importance of high momentum data

It is often assumed that high-order structure factors reflect only core contributions and are therefore inconsequential for describing the valence charge density. Figure 4 shows the refined population parameter P_{40}(Ni) at HT for a range of increasing momentum cutoff values. Here, only P_{40}(Ni) and P_{40}(O) were allowed to vary, with the other parameters being fixed to their optimum values derived from the complete data set. The progressive convergence towards a plateau clearly demonstrates that high momentum Fourier components are sensitive to the valence deformation and affect the ensuing accuracy, thus disproving the assertion that only very few reflections are of importance in reproducing the asphericity of the electron density. Despite the extreme accuracy of the low-order reflections (see Table III), one is still left with an ill-defined deformation parameter for the case that solely these data are used.

It should be pointed out in this context that the convergent beam electron diffraction measurements by Dudarev *et al.*[1] were complete only up to $\sin\theta/\lambda=0.5$ Å^{-1} (i.e., the six low-order data from Table III), and included one further datum at $\sin\theta/\lambda=0.68$ Å^{-1}. The inability to measure precise high order data appears to be a severe limitation to the ability to accurately characterize $\rho(\mathbf{r})$, as argued in the Introduction.

VII. SUMMARY

A detailed investigation of electron-density distribution in paramagnetic and antiferromagnetic NiO has been presented. Though NiO has been regarded over the years as the prototype member of the late 3*d* transition metal monoxides, the effect of magnetic order on the electron density differs radically from that found in MnO and CoO. Drastic rearrangement of the electron density has been observed for the latter compounds, whereas no significant influence appears to occur in NiO. Another important difference includes the behavior of the e_g subshell. Other important findings of the present study are the following: (i) The 3*d* valence shell is contracted by 3%, and the oxygen shell shows a corresponding expansion; (ii) a reduced spin magnetic moment and unquenched orbital moment are found on Ni; (iii) the Ni-O interaction is evidenced as purely ionic.

ACKNOWLEDGMENTS

We thank Dr. H.-J. Bleif for helpful discussions and support, and H. O. Sørensen for evaluation of the AIM charges.

[1] S. L. Dudarev, L.-M. Peng, S. Y. Savrasov, and J.-M. Zuo, Phys. Rev. B **61**, 2506 (2000).
[2] W. Jauch and M. Reehuis, Phys. Rev. B **65**, 125111 (2002).
[3] W. Jauch and M. Reehuis, Phys. Rev. B **67**, 184420 (2003).
[4] W. Jauch, J. Phys. Chem. Solids **62**, 2103 (2001).
[5] L. C. Bartel and B. Morosin, Phys. Rev. B **3**, 1039 (1971).
[6] *Computer Code XTAL 3.4, User's Manual*, edited by S. R. Hall, G. S. D. King, and J. M. Stewart (University of Western Australia, Perth, Australia, 1995).
[7] E. F. Skelton and J. L. Katz, Acta Crystallogr., Sect. A: Cryst. Phys., Diffr., Theor. Gen. Crystallogr. **A25**, 319 (1969).
[8] R. F. S. Hearmon, in *Numerical Data and Functional Relationships in Science and Technology*, edited by K.-H. Hellwege, Landolt-Börnstein New Series, Group III (Springer-Verlag, Berlin, 1979), Vol. 11.
[9] R. F. Stewart, M. Spackman, and C. Flensburg, *Computer Code VALRAY, User's Manual* (Carnegie-Mellon University, Pittsburgh, Pennsylvania, and University of Copenhagen, Copenhagen, Denmark, 2000).
[10] E. Clementi and C. Roetti, At. Data Nucl. Data Tables **14**, 177 (1974).
[11] P. J. Becker and P. Coppens, Acta Crystallogr., Sect. A: Cryst. Phys., Diffr., Theor. Gen. Crystallogr. **31**, 417 (1975).
[12] W. L. Roth, Acta Crystallogr. **13**, 140 (1960).
[13] R. F. Stewart, Acta Crystallogr., Sect. A: Cryst. Phys., Diffr., Theor. Gen. Crystallogr. **32**, 565 (1976).
[14] R. F. W. Bader, *Atoms in Molecules: A Quantum Theory* (Clarendon, Oxford, 1990).
[15] Yu. A. Abramov, Acta Crystallogr., Sect. A: Found. Crystallogr. **A53**, 264 (1997).
[16] D. Cremer and E. Kraka, Angew. Chem., Int. Ed. Engl. **23**, 67 (1984).
[17] D. Cremer and E. Kraka, Croat. Chem. Acta **57**, 1259 (1984).
[18] C. Flensburg and D. Madsen, Acta Crystallogr., Sect. A: Found. Crystallogr. **A56**, 24 (2000).
[19] J. Meister and W. H. E. Schwarz, J. Phys. Chem. **98**, 8245 (1994).
[20] C. Huiszoon and P. P. M. Groenewegen, Acta Crystallogr., Sect. A: Cryst. Phys., Diffr., Theor. Gen. Crystallogr. **A28**, 170 (1972).
[21] H. X. Gao, L.-M. Peng, and J. M. Zuo, Acta Crystallogr., Sect. A: Found. Crystallogr. **A55**, 1014 (1999).
[22] J. van Elp, H. Eskes, P. Kuiper, and G. A. Sawatzky, Phys. Rev. B **45**, 1612 (1992).
[23] H. A. Alperin, Phys. Rev. Lett. **6**, 55 (1961).
[24] M. Blume, Phys. Rev. **124**, 96 (1961).
[25] D. C. Khan, S. M. Kirtane, and J. K. Sharma, Phys. Rev. B **23**, 2697 (1981).
[26] A. Holladay, P. Leung, and P. Coppens, Acta Crystallogr., Sect. A: Cryst. Phys., Diffr., Theor. Gen. Crystallogr. **A38**, 563 (1982).
[27] W. E. Pickett, S. C. Erwin, and E. C. Ethridge, Phys. Rev. B **58**, 1201 (1998).
[28] V. Fernandez, C. Vettier, F. de Bergevin, C. Giles, and W. Neubeck, Phys. Rev. B **57**, 7870 (1998).
[29] S. K. Kwon and B. I. Min, Phys. Rev. B **62**, 73 (2000).
[30] A. Abragam and B. Bleaney, *Electron Paramagnetic Resonance of Transition Ions* (Clarendon, Oxford, 1970).
[31] A. K. Cheetham and D. A. O. Hope, Phys. Rev. B **27**, 6964 (1983).
[32] M. T. Hutchings and E. J. Samuelsen, Phys. Rev. B **6**, 3447 (1972).
[33] L. V. Dobysheva, P. L. Potapov, and D. Schryvers, Phys. Rev. B **69**, 184404 (2004).
[34] C. F. Bunge, J. A. Barrientos, and A. V. Bunge, At. Data Nucl. Data Tables **53**, 113 (1993).
[35] Z. Su and P. Coppens, Acta Crystallogr., Sect. A: Found. Crystallogr. **A54**, 646 (1998).
[36] L. Kissel, B. Zhou, S. C. Roy, S. K. S. Gupta, and R. H. Pratt, Acta Crystallogr., Sect. A: Found. Crystallogr. **A51**, 271 (1995).
[37] D. Schaupp, M. Schmacher, F. Smend, and P. Rullhusen, J. Phys. Chem. Ref. Data **12**, 467 (1983).
[38] *International Tables for Crystallography*, 2nd ed., edited by A. J. C. Wilson and E. Prince (Kluwer Academic, Dordrecht, 1999), Vol. C.